*Astronomy & Astrophysics* manuscript no. pe19˙v2
June 12, 2012


# Measurement of acoustic glitches in solar-type stars observed by *Kepler*

A. Mazumdar[1], M. J. P. F. G. Monteiro[2,3], J. Ballot[4,5], H. M. Antia[6], S. Basu[7], G. Houdek[8,9], S. Mathur[10], M. S. Cunha[2], V. Silva Aguirre[11,9], R. A. García[12], D. Salabert[13], G. A. Verner[12], H. Bruntt[9], J. Christensen-Dalsgaard[9], M. J. Thompson[10], T. S. Metcalfe[10], T. Appourchaux[14], and W. J. Chaplin[15]

[1] Homi Bhabha Centre for Science Education, TIFR, V. N. Purav Marg, Mankhurd, Mumbai 400088, India
[2] Centro de Astrofísica da Universidade do Porto, Rua das Estrelas, 4150-762 Porto, Portugal
[3] Departamento de Física e Astronomia, Faculdade de Ciências da Universidade do Porto, Rua do Campo Alegre, 4169-007 Porto, Portugal
[4] CNRS, Institut de Recherche en Astrophysique et Planétologie, 14 avenue Edouard Belin, 31400 Toulouse, France
[5] Université de Toulouse, UPS-OMP, IRAP, 31400 Toulouse, France
[6] Tata Institute of Fundamental Research, Homi Bhabha Road, Mumbai 400005, India
[7] Astronomy Department, Yale University, P.O. Box 208101, New Haven, CT 065208101, USA
[8] Institute of Astronomy, University of Vienna, 1180, Vienna, Austria
[9] Department of Physics and Astronomy, Aarhus University, 8000 Aarhus C, Denmark
[10] High Altitude Observatory, NCAR, P.O. Box 3000, Boulder, CO 80307, USA
[11] Max Planck Institut für Astrophysik, Karl-Schwarzschild-Str. 1, 85748, Garching bei München, Germany
[12] Laboratoire AIM, CEA/DSM, CNRS, Université Paris Diderot, IRFU/SAp, Centre de Saclay, 91191 Gif-sur-Yvette Cedex, France
[13] Université de Nice Sophia-Antipolis, CNRS, Observatoire de la Côte d'Azur, BP 4229, 06304 Nice Cedex 4, France
[14] Institut d'Astrophysique Spatiale, UMR8617, Université Paris XI, Batiment 121, 91405 Orsay Cedex, France
[15] School of Physics and Astronomy, University of Birmingham, Edgbaston, Birmingham, B15 2TT, UK

**ABSTRACT**

The oscillatory signal in the frequencies caused by the presence of layers of sharp variation in sound speed in stellar interiors is used to determine the acoustic locations of such layers in 19 solar-type stars observed by the *Kepler* mission. The presence of this signal in the frequencies themselves, the second differences of frequencies and the ratio of small to large separation was utilised by four independent groups of researchers to locate the base of the convection zone and the second helium ionisation zone. Despite the significantly different methods of analysis, remarkable agreement was found between the results of these four groups. Further, the extracted locations of these layers were found to be consistent with representative models of the stars. This firmly establishes the presence of the oscillatory signal in the seismic data and the viability of several techniques to use it to determine the location of acoustic glitches inside stars.

**Key words.** stars: oscillations – stars: interiors

## 1. Introduction

Acoustic glitches in a star are the regions where the sound speed undergoes an abrupt variation due to a localised sharp change in the stratification. The major acoustic glitches are the boundaries between radiative and convective regions and the layers of ionisation of elements, especially hydrogen and helium. Such a glitch introduces an oscillatory component in the eigenfrequencies of the star with respect to the frequencies themselves, proportional to $\sin(4\pi\tau_{\rm g}\nu_{n,l}+\phi)$ (Gough 1990), where $\tau_{\rm g}=\int_{r_{\rm g}}^{R_{\rm s}}\frac{{\rm d}r}{c}$ is the acoustic depth of the glitch measured from the surface, $c$ the speed of sound, $r_{\rm g}$ the radial distance of the glitch, $R_{\rm s}$ the seismic radius of the star (see discussion below), $\nu_{n,l}$ the frequency of a mode with radial order $n$ and degree $l$, and $\phi$ a phase factor. Each glitch will contribute to such a signal in the frequencies with a "periodicity" of the corresponding acoustic depth.

This oscillatory signature has been extensively studied for the Sun in order to determine the extent of overshoot below the solar convection zone (Gough 1990; Gough & Sekii 1993; Monteiro et al. 1994; Basu et al. 1994; Roxburgh & Vorontsov 1994; Basu 1997). It has been proposed earlier that this may be used for distant stars also to find the position of the base of the convective envelope or the second helium ionisation zone (Monteiro et al. 2000; Mazumdar & Antia 2001; Gough 2002; Roxburgh & Vorontsov 2003; Ballot et al. 2004; Basu et al. 2004; Houdek 2004; Houdek & Gough 2004, 2007; Mazumdar 2005). Indeed, Miglio et al. (2010) have used the modulation of the frequency separations to determine the location of the second helium ionisation zone in a red giant star. Recently, Mazumdar et al. (2012) have used the oscillatory signal in the second differences of the frequencies of a solar-type star observed with CoRoT to determine the acoustic depth of its second helium ionisation zone and the base of the convective envelope.

The scientific interest in studying the acoustic glitches goes beyond the obvious goal of placing constraints on the positions of specific layers in the stellar interior The accurate determination of the location of the base of the convective envelope, for example, will help us refine our understanding of the stellar dynamo in cool stars. On the other hand, the amplitude of the oscillatory signal from the ionisation zones is directly related to the

*Send offprint requests to*: anwesh@tifr.res.in

abundance of the corresponding element in the star. For helium especially, an estimate of the helium abundance in an ensemble of stars of different masses and ages will lead us to a better understanding of the process of element enrichment in stars which can be extrapolated back to the primordial helium content of the universe, an important parameter in cosmology.

In the present analysis we studied 19 stars continuously observed by the *Kepler mission* (Borucki et al. 2010; Koch et al. 2010) during 9 continuous months. Launched on 2009 March 7 (UTC), *Kepler* is monitoring 150 000 stars of the constellation of Cygnus every half an hour to look for Earth-like planets orbiting around solar-like stars. Photometric time series of a subsample of 512 stars are studied at a shorter cadence of 58.84876 s (Gilliland et al. 2010). Every 3 months the spacecraft rolls by 90°, to maintain the solar panels directed towards the Sun and the radiator that cools down the focal plane out of the solar light. Therefore, the datasets are organised in quarters. The time series of our sample of 19 stars were acquired during quarters 5 to 9, processed following the methods described in García et al. (2011), and their frequencies extracted as described in Appourchaux et al. (2012).

In the next section we describe in detail the different techniques used to determine the location of the acoustic glitches. In Sect. 3 we present the results of our study and discuss them in Sect. 4. We summarise the conclusions in Sect. 5.

## 2. The techniques

We applied four different methods (labelled A to D below) to determine the acoustic locations of the base of the convective zone (BCZ) and the second helium ionisation zone (HeIIZ). The different methods were applied on the same input data, namely the *Kepler* frequencies of the stars, by different subsets of the present authors independently, and the final results are compared in Sec. 3.

The first method (Method A) utilises the oscillatory signals in the frequencies themselves. Methods B and C both fit functional forms to the second differences of the frequencies with $\tau_{\rm BCZ}$ and $\tau_{\rm HeIIZ}$ among the free parameters, but have important differences in the fitting forms. Finally, method D utilises the oscillatory signal present in the ratio of the small to the large separation.

In the rest of the paper, we adopt the following notations for the acoustic depth (measured from the surface) and radii (measured from the centre): $\tau_{\rm BCZ}$ and $\tau_{\rm HeIIZ}$ for the acoustic depths of BCZ and HeIIZ, respectively; $T_{\rm BCZ}$ and $T_{\rm HeIIZ}$ for the acoustic radii, respectively. $T_0$ is the total acoustic radius of the star, which can be calculated as

$$T_0 = \int_0^{R_{\rm s}} {\rm d}r/c\,, \qquad (1)$$

where $c$ is the speed of sound. $R_{\rm s}$ is the seismic radius of the star, which may be considered as a fiducial radius that defines the outer phase of the acoustic modes, subject to the chosen boundary conditions, relatively to the phase in the propagating region below the turning point. $R_{\rm s}$ can be determined from fitting an approximated atmosphere, such as an polytropic atmosphere, to a more realistic stellar atmosphere (such as that obtained from 3D numerical simulations or from observations). In the case of the Sun this fiducial radius is beyond the temperature minimum, i.e., rather far away from the photosphere (about 225 s above the radius corresponding to the effective temperature). The total acoustic radius can also be estimated from the average large separation, $\Delta_0$, as $T_0 \approx (2\Delta_0)^{-1}$.

In Figs. 1 to 4, we illustrate each of the four methods, as applied to some *Kepler* stars. A more detailed discussion on these results is given in the next section.

### 2.1. Method A

In this method the strategy is to isolate the signature of the acoustic glitches in the frequencies themselves. Compared to the method involving second differences, described in Sects. 2.2 and 2.3, this is less sensitive to uncertainties, does not require having frequencies of consecutive order and avoids the additional terms that need to be considered when fitting the expression to frequency differences. However it is less robust on the convergence to a valid solution (the starting point must be sufficiently close to the solution) as we do not put any constraints on what we consider to be a smooth component of the frequencies.

Here we assume that only very low-degree data are available so that any dependence on mode degree can be ignored. The expression for the signature due to the BCZ is taken from Monteiro et al. (1994), Christensen-Dalsgaard et al. (1995), and Monteiro et al. (2000). The expression for the signature due to the HeIIZ is from Monteiro & Thompson (1998) and Monteiro & Thompson (2005), with some minor adaptations and/or simplifications.

In the following $\nu_r$ is a reference frequency, introduced for normalising the amplitude. One good option would be to use $\nu_r = \nu_{\rm max}$ (frequency of maximum power), but the actual value selected is not relevant unless we want to compare the amplitude of the signal of different stars.

The signal from the BCZ, after removing a smooth component from the frequencies, is written as

$$\delta\nu_{\rm BCZ} \simeq A_{\rm BCZ}\left(\frac{\nu_r}{\nu}\right)^2 \cos(4\pi\tau_{\rm BCZ}\nu + 2\phi_{\rm BCZ})\,. \qquad (2)$$

The parameters to be determined in this expression are $A_{\rm BCZ}$, $\tau_{\rm BCZ}$, $\phi_{\rm BCZ}$ for amplitude, acoustic depth and phase, respectively. The typical values to expect for a solar-like star are $A_{\rm BCZ} \sim 0.1\,\mu$Hz, $\tau_{\rm BCZ} \sim 2300$ s and $\phi_{\rm BCZ} \sim \pi/4$.

The signal from HeIIZ, after removing a smooth component from the frequencies, is described by

$$\delta\nu_{\rm HeIIZ} \simeq A_{\rm HeIIZ}\left(\frac{\nu_r}{\nu}\right)\sin^2(2\pi\beta_{\rm HeIIZ}\,\nu)\cos(4\pi\tau_{\rm HeIIZ}\nu + 2\phi_{\rm HeIIZ})\,. \qquad (3)$$

The free parameters in this expression are $A_{\rm HeIIZ}$, $\beta_{\rm HeIIZ}$, $\tau_{\rm HeIIZ}$, $\phi_{\rm HeIIZ}$ corresponding, respectively, to amplitude, acoustic width, acoustic depth and phase. The typical values to expect for a solar-like star for these parameters are $A_{\rm HeIIZ} \sim 1.0\,\mu$Hz, $\beta_{\rm HeIIZ} \sim 130$ s, $\tau_{\rm HeIIZ} \sim 700$ s and $\phi_{\rm HeIIZ} \sim \pi/4$.

If low-degree frequencies are used for a solar-type star, then the signals present in the data correspond to having

$$\nu = \nu_{\rm s1} + \delta\nu_{\rm HeIIZ} + \delta\nu_{\rm BCZ} \qquad \text{or} \qquad \nu = \nu_{\rm s2} + \delta\nu_{\rm BCZ}\,, \qquad (4)$$

where $\nu_{si}$ ($i = 1, 2$) is a "smooth" component of the mode frequency to be removed. The parameters to fit these expressions are for Eq. 2 (BCZ): $A_{\rm BCZ}$, $\tau_{\rm BCZ}$, $\phi_{\rm BCZ}$; and for Eq. 3 (HeIIZ): $A_{\rm HeIIZ}$, $\beta_{\rm HeIIZ}$, $\tau_{\rm HeIIZ}$, $\phi_{\rm HeIIZ}$ (in this case we treat $\delta\nu_{\rm BCZ}$ as noise).

The fitting procedure used is the same method as described by Monteiro et al. (2000). This method uses an iterative process in order to remove the slowly varying trend of the frequencies, leaving the required signature given in either Eq. (2) or Eq. (3). A polynomial in $n$ is fitted to the frequencies of all modes of given degree $l$ separately, using a regularised least-squares fit with third-derivative smoothing through a parameter $\lambda_0$ (see Monteiro et al. (1994) for the details). The residuals to

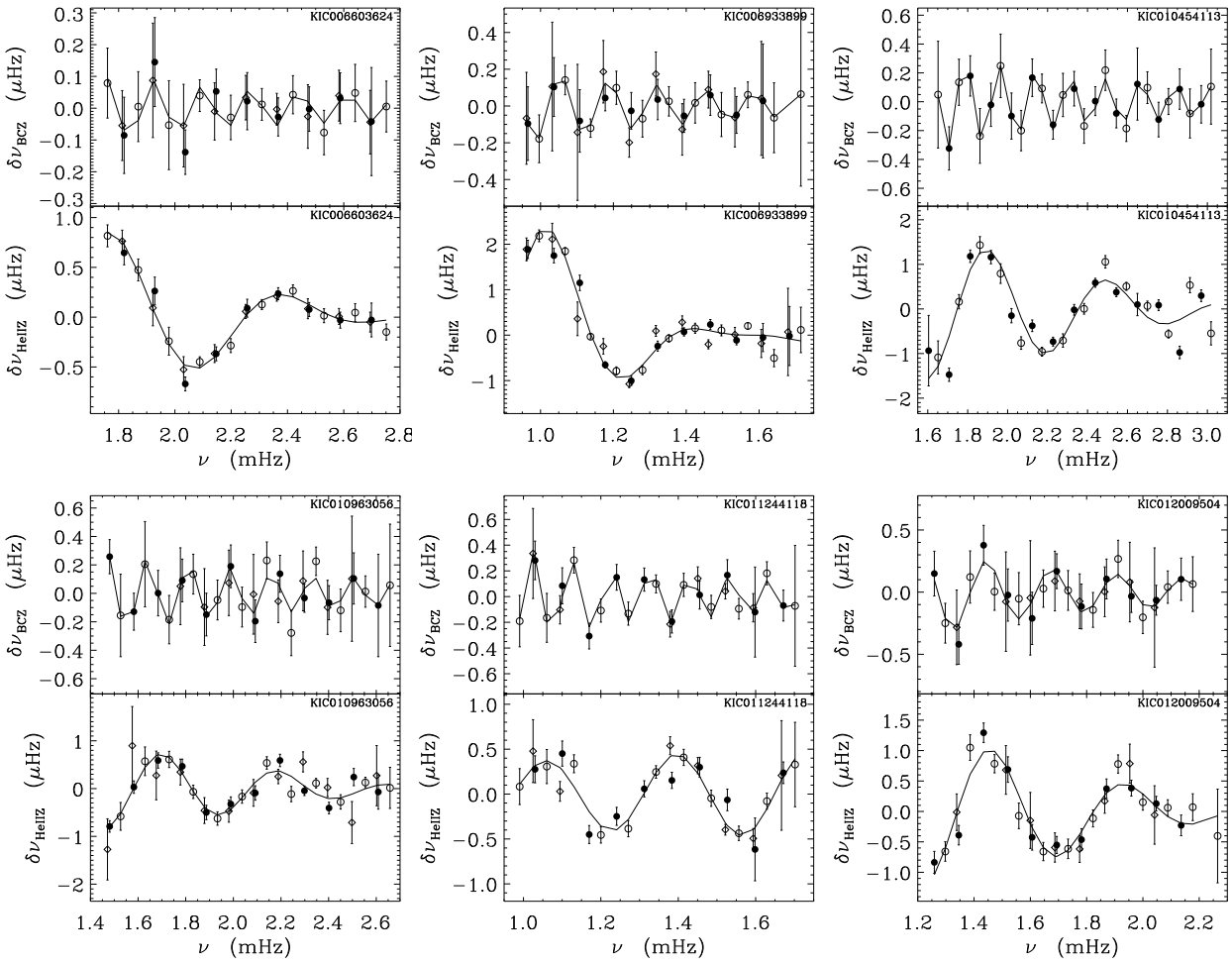


**Fig. 1.** Illustration of method A: Fits of Eqs. 2 and 3 to the residuals of frequencies of six *Kepler* stars (KIC numbers given in each panel) after removing a smooth component iteratively. The points correspond to $l = 0$ (black circles), $l = 1$ (open circles) and $l = 2$ (diamonds), while the *solid line* is the best fit to the BCZ component (Eq. 2, *upper panel* for each star) and the HeIIZ component (Eq. 3, *lower panel* for each star).

those fits are then fitted for all degrees simultaneously. The latter fit is the "signal" either from the BCZ or from the HeIIZ. This procedure is then iterated (by decreasing the smoothing): at each iteration we remove from the frequencies the previously fitted signal and recalculate the smooth component of the frequencies this time using the smaller value of $\lambda_n$ ($n = 1, 2, 3, ..$). The iteration converges when there are no changes to the smooth component or the signal (typically it goes up to $n \simeq 3$).

The initial smoothing, selected through the parameter $\lambda_0$, defines the range of wavelengths whose variation we want to isolate. To isolate the signature from the BCZ, a smaller initial value of $\lambda_0$ is required in order to ensure that the smooth component also extracts the signature from the HeIIZ. However, when isolating the signature from the HeIIZ, the shorter wavelength signature from the BCZ is also retained.

We show the fits to Eqs. 2 and 3 in Fig. 1 for six of the *Kepler* stars that we studied.

In order to estimate the impact on the fitting of the observational uncertainties we use Monte Carlo simulations. We do so by producing sets of frequencies calculated from the observed values with added random values calculated from a standard normal distribution multiplied by the quoted observational uncertainty. In the fit we remove frequencies with large errors ($> 0.5\,\mu$Hz for the BCZ and $> 1.0\,\mu$Hz for the HeIIZ). For each star we produce 500 sets of frequencies, determining the parameters as the standard deviation of the results for the parameters. Only valid fits are used, as long as the number of valid fits represent more than 90% of the simulations. Otherwise we consider that the signature has not been fit successfully (even if a solution can be found for the observations).

### 2.2. Method B

This method involves the second differences of the frequencies to determine $\tau_{\rm BCZ}$ and $\tau_{\rm HeIIZ}$ simultaneously by fitting a functional form to the oscillatory signals.

The oscillatory signal in the frequencies due to an acoustic glitch is quite small and is embedded in the frequencies together with a smooth trend arising from the regular variation of the sound speed in the stellar interior. It can be enhanced by using the second differences

$$\Delta_2\nu(n,l) = \nu(n-1,l) - 2\nu(n,l) + \nu(n+1,l), \quad (5)$$

instead of the frequencies $\nu(n,l)$ themselves (see, e.g., Gough 1990; Basu et al. 1994; Mazumdar & Antia 2001; Basu et al. 2004).

We fit the second differences to a suitable function representing the oscillatory signals from the two acoustic glitches (Mazumdar & Antia 2001). We adopt the following functional form which has been adapted from Houdek & Gough (2007)

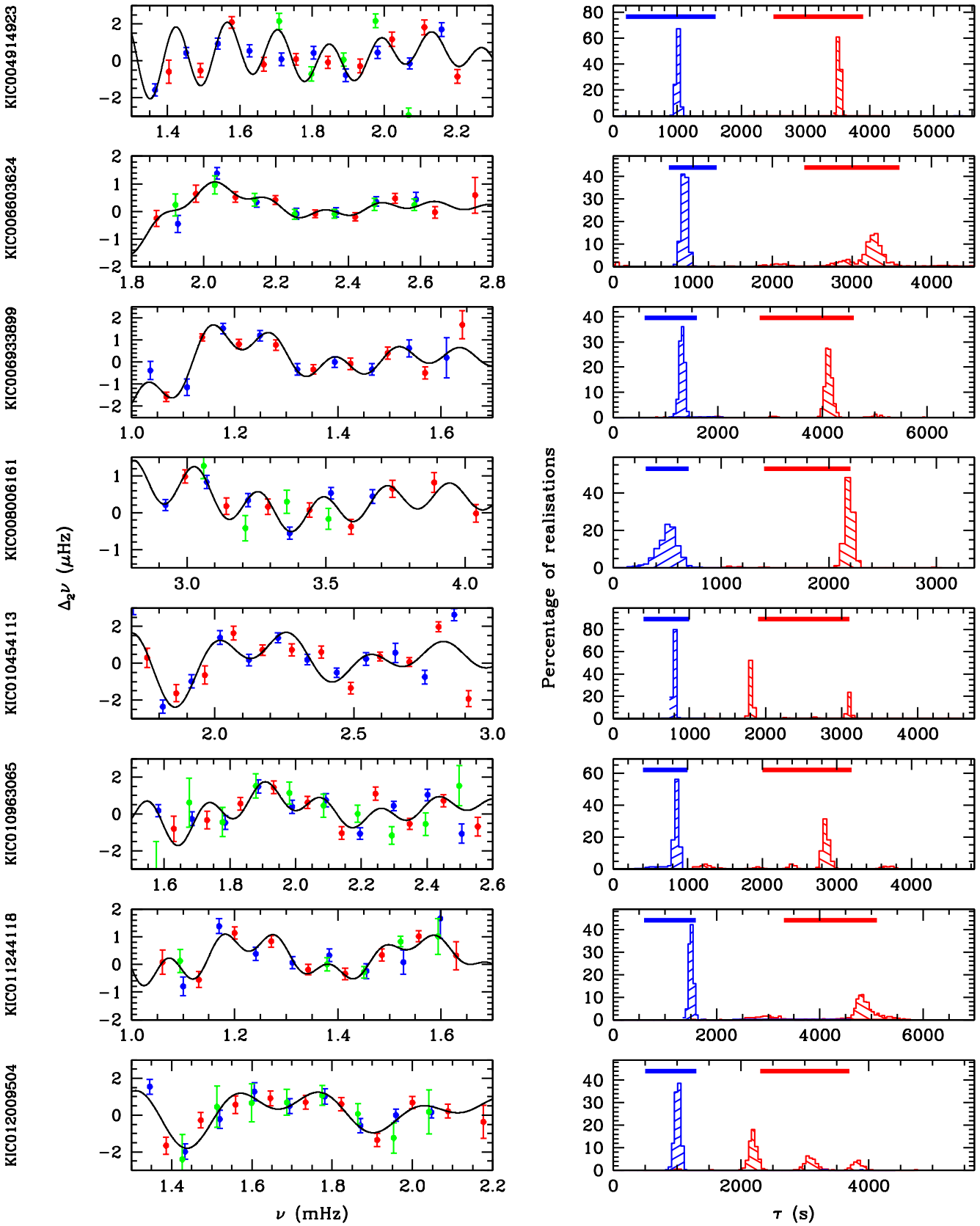


**Fig. 2.** Illustration of method B: Fits of Eq. 6 to the second differences of the mean frequencies for eight *Kepler* stars (KIC numbers on the *extreme left*) and the histograms for the fitted values of $\tau_{\rm HeIIZ}$ and $\tau_{\rm BCZ}$ for different realisations of the data. The second differences of the frequencies of $l = 0$ (*blue*), $l = 1$ (*red*) and $l = 2$ (*green*) modes of the stars and their fit to Eq. 6 (*black curve*) are shown in the *left* panels. The corresponding histograms of the fitted values of $\tau_{\rm BCZ}$ (in *red*) and $\tau_{\rm HeIIZ}$ (in *blue*) for different realisations are shown in the *right* panels. The *solid* bands at the top of the *right panels* indicate the range of initial guesses for the two parameters in each fit.

(Eq. (22) therein).

$$\begin{aligned}\Delta_2\nu \;=\; & a_0 \\ & +(b_2/\nu^2)\sin(4\pi\nu\tau_{\rm BCZ}+2\phi_{\rm BCZ}) \\ & +(c_0\nu\exp(-c_2\nu^2))\sin(4\pi\nu\tau_{\rm HeIIZ}+2\phi_{\rm HeIIZ}),\end{aligned} \tag{6}$$

where $a_0$, $b_2$, $c_0$, $c_2$, $\tau_{\rm BCZ}$, $\phi_{\rm BCZ}$, $\tau_{\rm HeIIZ}$ and $\phi_{\rm HeIIZ}$ are 8 free parameters of fitting. For one of the stars in our set (KIC010018963), we need to use a slightly different function in which the constant term representing the smooth trend, $a_0$, is replaced by a parabolic form: $(a_0 + a_1\nu + a_2\nu^2)$. Although this parabolic form can, in principle, be used for all stars as well, it actually interferes with the slowly varying periodic HeIIZ component in the limited range of observed frequencies, and makes it difficult to determine $\tau_{\rm HeIIZ}$. Therefore, in adopting Eq. (6) we essentially assume that the smooth trend in the frequencies has been reduced to a constant shift in the process of taking the second differences. We ignore frequencies which have errors of more than 1 $\mu$Hz.

While Eq. 6 is not the exact form prescribed by Houdek & Gough (2007), it captures the essential elements of that form while keeping the number of free parameters relatively small. The ignored terms can be shown to have relatively smaller contributions. We note that Basu et al. (2004) have shown that the exact form of the amplitudes of the oscillatory signal does not affect the results significantly. The fits of Eq. 6 to the second differences of some selected stars in our sample are shown in the *left* panels of Fig. 2.

The fitting procedure is similar to the one described by Mazumdar et al. (2012). The fit is carried out through a non-linear $\chi^2$ minimisation, weighted by the errors in the data. The correlation of errors in the second differences is accounted for by defining the $\chi^2$ using a covariance matrix. The effects of the errors are considered by repeating the fit for 1000 realisations of the data, produced by skewing the frequencies by random errors corresponding to a normal distribution with standard deviation equal to the quoted $1\sigma$ error in the frequencies. The successful convergence of such a non-linear fitting procedure is somewhat dependent on the choice of reasonable initial guesses. To remove the effect of initial guesses affecting the final fitted parameters, we carry out the fit for multiple combinations of starting values. For each realisation, the fitting is repeated for 100 random combinations of initial guesses of the free parameters and the fit which produces the minimum value of $\chi^2$ is accepted.

The median value of each parameter for 1000 realisations is taken as its fitted value. The $\pm1\sigma$ error in the parameter is estimated from the range of values covering 34% area about the median in the histogram of fitted values. Thus the quoted errors in these parameters reflect the width of these histograms on two sides of the median value. The histograms for $\tau_{\rm BCZ}$ and $\tau_{\rm HeIIZ}$ and the ranges of initial guesses of the corresponding parameters are shown in the *right* panels of Fig. 2.

In some cases the fitting of the $\tau_{\rm BCZ}$ parameter suffers from the aliasing problem (Mazumdar & Antia 2001), where a significant fraction of the realisations are fitted with $\tau_{\rm BCZ}$ equal to $\tilde{\tau}_{\rm BCZ} \equiv T_0 - \tau_{\rm BCZ}$. This becomes apparent from the histogram of $\tau_{\rm BCZ}$ which appears bimodal with a reflection around $T_0/2$ (e.g., for KIC10454113, shown in Fig. 2). In such cases, we choose the higher peak in the histogram to represent the true value of $\tau_{\rm BCZ}$, and the error in the parameter is calculated after "folding" the histogram about the acoustic mid-point $T_0/2$, the acoustic radius being estimated from the mean large separation, $\Delta_0$. For a few stars there are multiple peaks in the histogram for $\tau_{\rm BCZ}$, not all of which can be associated with the true depth of the BCZ or its aliased value (e.g., for KIC12009504, shown in *bottom right* panel of Fig. 2). In such cases we choose only the most prominent peak to determine the median and the error is estimated from the width of that peak. The remaining realisations are also neglected for estimating the other parameters such as $\tau_{\rm HeIIZ}$.

### 2.3. Method C

Approximate expressions for the frequency contributions $\delta\nu_i$ arising from acoustic glitches in solar-type stars were recently presented by Houdek & Gough (2007, 2011), which we adopt here for producing the results presented in Fig. 3 and Table 2. A detailed discussion of the method can be found in those references; we therefore present here only a summary. The complete expression for $\delta\nu_i$ is given by

$$\delta\nu_i = \delta_\gamma\nu_i + \delta_{\rm c}\nu_i + \delta_{\rm u}\nu_i\,, \tag{7}$$

where the three terms on the RHS represent acoustic glitches from three different sources inside the star.

The first term,

$$\begin{aligned}\delta_\gamma\nu \;=\; & -\sqrt{2\pi}A_{\rm II}\Delta_{\rm II}^{-1}\left[\nu+\tfrac{1}{2}(m+1)\Delta_0\right] \\ & \times\Bigg[\tilde{\mu}\tilde{\beta}\int_0^{T_0}\kappa_{\rm I}^{-1}{\rm e}^{-(\tau-\tilde{\eta}\tau_{\rm II})^2/2\tilde{\mu}^2\Delta_{\rm II}^2}|x|^{1/2}|{\rm Ai}(-x)|^2\,{\rm d}\tau \\ & +\int_0^{T_0}\kappa_{\rm II}^{-1}{\rm e}^{-(\tau-\tau_{\rm II})^2/2\Delta_{\rm II}^2}|x|^{1/2}|{\rm Ai}(-x)|^2\,{\rm d}\tau\Bigg]\end{aligned} \tag{8}$$

arises from the variation in $\gamma_1 = (\partial\ln p/\partial\ln\rho)_s$ ($p$ and $\rho$ are pressure and density respectively and $s$ is specific entropy) induced by helium ionisation. The constant $m = 3.5$ is a representative polytropic index in the expression for the approximate effective phase $\psi$ appearing in the argument of the Airy function ${\rm Ai}(-x)$, and $\tilde{\beta}$, $\tilde{\eta}$ and $\tilde{\mu}$ are constants of order unity which account for the relation between the acoustic glitches caused by the first (He I) and second (He II) stages of ionisation of helium (Houdek & Gough 2007); $\tau$ is acoustic depth beneath the seismic surface of the star; $\Delta_{\rm II}$ and $\tau_{\rm II} \equiv \tau_{\rm HeIIZ}$ are respectively the acoustic width of the He II glitch and its acoustic depth beneath the seismic surface. The argument of the Airy function is $x = {\rm sgn}(\psi)|3\psi/2|^{2/3}$, where

$$\psi(\tau) = \kappa\omega\tilde{\tau} - (m+1)\cos^{-1}[(m+1)/\omega\tilde{\tau}] \qquad \text{if } \tilde{\tau} > \tau_{\rm t}\,, \tag{9}$$

and

$$\psi(\tau) = |\kappa|\omega\tilde{\tau} - (m+1)\ln[(m+1)/\omega\tilde{\tau} + |\kappa|] \quad \text{if } \tilde{\tau} \le \tau_{\rm t}\,, \tag{10}$$

in which $\tilde{\tau} = \tau + \omega^{-1}\epsilon_{\rm II}$, with $\epsilon_{\rm II}$ ($\epsilon_{\rm I} = \epsilon_{\rm II}$) being a phase constant, and $\tau_{\rm t}$ is the location of the upper turning point of the mode; also $\kappa(\tau) = [1-(m+1)^2/\omega^2\tilde{\tau}^2]^{1/2}$, and $\kappa_{\rm I} = \kappa(\tilde{\eta}\tau_{\rm II})$ and $\kappa_{\rm II} = \kappa(\tau_{\rm II})$.

The second term in Eq. 7,

$$\begin{aligned}\delta_{\rm c}\nu \;\simeq\; & A_{\rm c}\Delta_0^3\nu^{-2}\left(1+1/16\pi^2\tau_0^2\nu^2\right)^{-1/2} \\ & \times\left\{\cos[2\psi_{\rm c}+\tan^{-1}(4\pi\tau_0\nu)]-(16\pi^2\tilde{\tau}_{\rm BCZ}^2\nu^2+1)^{1/2}\right\}\end{aligned} \tag{11}$$

arises from the acoustic glitch at the base of the convection zone resulting from a near discontinuity (a true discontinuity in theoretical models using local mixing-length theory with a non-zero mixing length at the lower boundary of the convection zone) in the second derivative of density. We model this acoustic glitch with a discontinuity in the squared acoustic cutoff frequency at $\tau_{\rm BCZ}$ coupled with an exponential relaxation in the radiative zone beneath, with acoustical scale time $\tau_0 = 80$ s, as did Houdek & Gough (2007, 2011). Further,

$$\psi_{\rm c} = \kappa_{\rm c}\omega\tilde{\tau}_{\rm BCZ} - (m+1)\cos^{-1}\left[(m+1)/\tilde{\tau}_{\rm BCZ}\omega\right] + \pi/4, \tag{12}$$

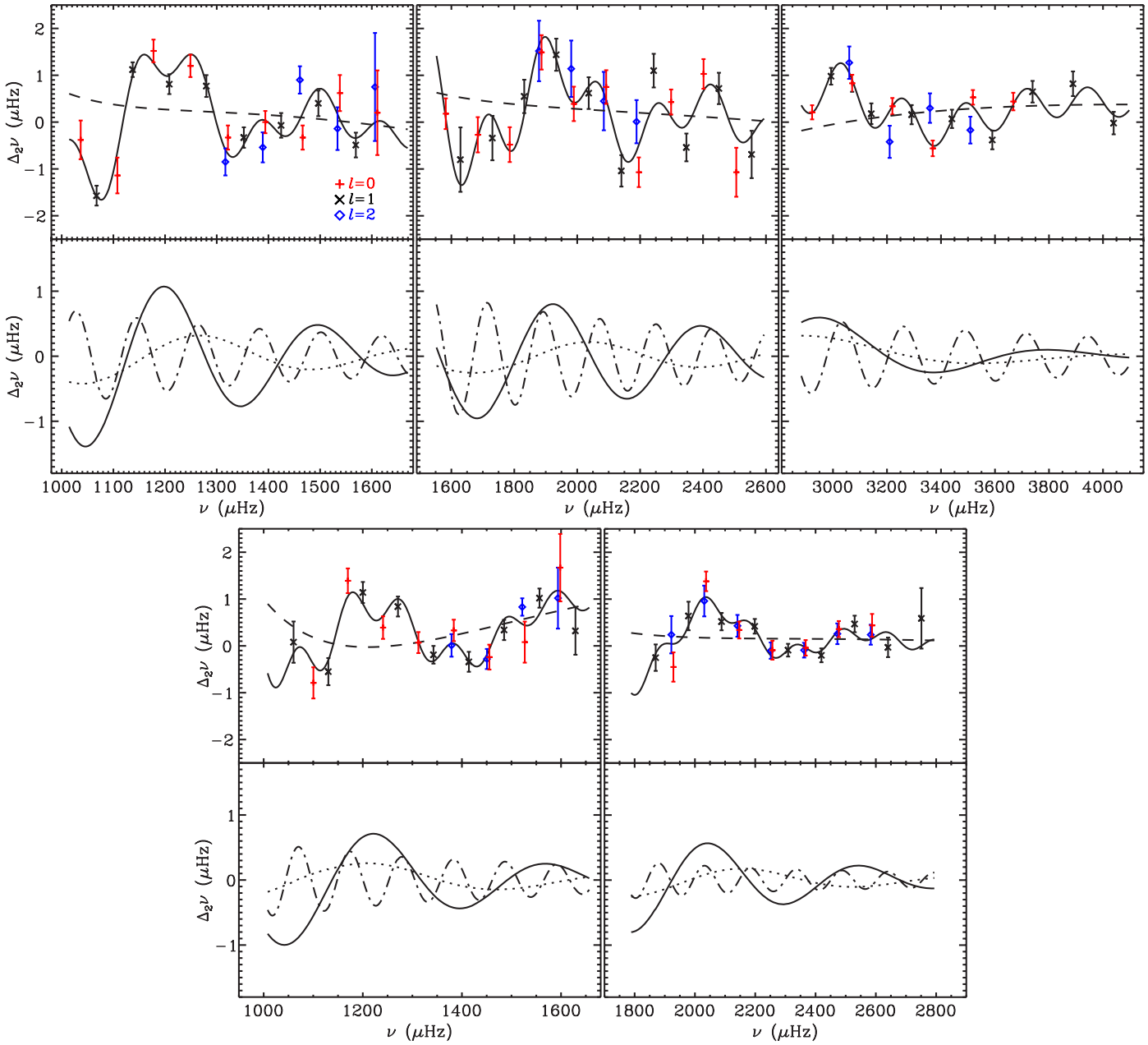


**Fig. 3.** Illustration of method C: Analyses results for KIC 6933899 (*top left*), KIC 10963065 (*top middle*), KIC 8006161 (*top right*), KIC 11244118 (*bottom left*) and KIC 6603624 (*bottom right*). The symbols in the *upper panels* denote second differences $\Delta_2\nu$ for low-degree modes. The solid curves are fits to $\Delta_2\nu$ based on the analysis by Houdek & Gough (2007, 2011). The dashed curves are the smooth contributions, including a third-order polynomial in $\nu_i^{-1}$ to represent the upper-glitch contribution from near-surface effects. The *lower panels* display the remaining individual contributions from the acoustic glitches to $\Delta_2\nu$: the *dotted* and *solid* curves are the contributions from the first and second stages of helium ionisation, and the *dot-dashed* curve is the contribution from the acoustic glitch at the base of the convective envelope.

where $\kappa_c = \kappa(\tau_{BCZ})$ and $\tilde{\tau}_{BCZ} = \tau_{BCZ} + \omega^{-1}\epsilon_c$.

The additional upper-glitch component $\delta_u\nu_i$, which is produced, in part, by wave refraction in the stellar core, by the ionisation of hydrogen and by the upper superadiabatic boundary layer of the envelope convection zone, is difficult to model. We approximate it as a series of inverse powers of $\nu$, truncated at the cubic order:

$$\Delta_2\delta_u\nu_i = \sum_{k=0}^{3} a_k \nu_i^{-k} \,. \tag{13}$$

The eleven coefficients $\eta_\alpha = (A_{II}, \Delta_{II}, \tau_{HeIIZ}, \epsilon_{II}, A_c, \tau_{BCZ}, \epsilon_c, a_0, a_1, a_2, a_3)$, $\alpha = 1, ..., 11$, are found by fitting the second differences (cf. Eq. 5)

$$\begin{aligned}\Delta_{2i}\nu(n,l) &:= \nu(n-1,l) - 2\nu(n,l) + \nu(n+1,l) \\ &\simeq \Delta_{2i}(\delta_\gamma\nu + \delta_c\nu + \delta_u\nu) =: g_i(\nu_j;\eta_\alpha)\end{aligned} \tag{14}$$

to the corresponding observations by minimising

$$E_g = (\Delta_{2i}\nu - g_i)C^{-1}_{\Delta ij}(\Delta_{2j}\nu - g_j) \tag{15}$$

where $C^{-1}_{\Delta ij}$ is the $(i, j)$ element of the inverse of the covariance matrix $C_\Delta$ of the observational errors in $\Delta_{2i}\nu$, computed, perforce, under the assumption that the errors in the frequency data

$\nu_i$ are independent. The covariance matrix $C_{\eta\alpha\gamma}$ of the errors in $\eta_\alpha$ were established by Monte Carlo simulation.

We show the results from this method for five of the stars in our sample in Fig. 3 where the different oscillatory components in the second differences are explicitly shown.

### 2.4. Method D

Determinations of acoustic depths of glitches are biased by surface effects (e.g. Christensen-Dalsgaard et al. 1995). A way to remove such biases is to consider acoustic radii of the signatures. First, it is possible to perform posterior determinations of radii by comparing depths to the total acoustic radius of the star derived from the average large separation $\Delta_0$ (see Ballot et al. 2004); it is also possible to directly measure acoustic radii by considering the small separations $d_{01}$ and $d_{10}$ or the frequency ratios $r_{01}$ and $r_{10}$ as shown by Roxburgh & Vorontsov (2003).

We use the 3-point differences:

$$d_{01,n} = \frac{1}{2}(2\nu_{n,0} - \nu_{n-1,1} - \nu_{n,1}), \tag{16}$$

$$d_{10,n} = -\frac{1}{2}(2\nu_{n,1} - \nu_{n,0} - \nu_{n+1,0}) \tag{17}$$

and the corresponding ratios:

$$r_{01,n} = \frac{d_{01,n}}{\Delta\nu_{1,n}}, \quad r_{10,n} = \frac{d_{10,n}}{\Delta\nu_{0,n+1}}. \tag{18}$$

We denote by $d_{010}$ and $r_{010}$ the sets $\{d_{01}, d_{10}\}$ and $\{r_{01}, r_{10}\}$, respectively.

Using these variables, the main contributions of outer layers are removed (see Roxburgh 2005). The global trend of these variables give then an information on the core of the star (e.g. Silva Aguirre et al. 2011; Cunha & Brandão 2011). Nevertheless, the most internal glitches, such as the BCZ, also imprint their signatures over the global trend. Using solar data, Roxburgh (2009) shows that we can recover the acoustic radius of the BCZ ($T_{\rm BCZ}$) by the use of a Fourier transform on the residuals obtained after removing the global trend. As a counterpart of this approach, information about surface layers, including He I and He II ionisation zones, are lost.

We use an approach similar to Roxburgh (2009) and develop a semi-automatic pipeline which extracts glitches from a frequency table of $l = 0$ and 1 modes. Instead of fitting a background first, then making a Fourier transform, we do both simultaneously by fitting the variable $y = \nu^* r_{010}$ (or $y = \nu^* d_{010}$) with the following expression:

$$f(\nu) = \sum_{k=0}^{m} \frac{c_k}{(\nu + \nu_{\rm r})^k} + A\sin(4\pi T\nu + \phi), \tag{19}$$

where $\nu^* = \nu/\nu_{\rm r}$ and $\nu_{\rm r}$ is a reference frequency. We have $m + 3$ free parameters: $\{c_k\}$, $A$, $T$, and $\phi$.

To be able to estimate reliable errors for $T_{\rm BCZ}$ we perform a Markov Chain Monte Carlo (MCMC) to fit the data. Our MCMC fitting algorithm is close to the one described, for example, in Benomar et al. (2009) or Handberg & Campante (2011), but without parallel tempering. Moreover, in our case the noise is not multiplicative and exponential, but additive and normal. We fix $m = 2$ and $\nu_{\rm r} = 0.8\nu_{\rm max}$, similar to the value adopted for the Sun by Roxburgh (2009). We use uniform priors for $A$, $T$ and $\phi$. The prior for $A$ is very broad (between 0 and $10\max(|y|)$; $\phi$ is $2\pi$-periodic with a uniform prior over $[0, 2\pi]$, and $T$ is restricted to $[\delta T, T_0 - \delta T]$, where $\delta T = (\max(\nu) - \min(\nu))^{-1}$. To determine priors for $\{c_k\}$, we first perform a standard linear least-square fitting without including the oscillatory component. Once we get the fitted values $\tilde{c}_k$ and associated errors $\sigma_k$, we use for $c_k$ priors which are uniform over $[\tilde{c}_k - 3\sigma_k, \tilde{c}_k + 3\sigma_k]$ with Gaussian decay around this interval. After a 200 000-iteration learning phase (the learning method we use is based on Benomar et al. 2009), MCMC is run for $10^7$ iterations. We test the convergence by verifying the consistence of results obtained by using the first and second half of the chain.

Posterior probability distributions (PDF) for $T$ are plotted for different stars in Fig. 4. Some PDFs exhibit a unique and clear mode that we attribute to the BCZ. $T_{\rm BCZ}$ is then estimated as the median of the distribution and 1-$\sigma$ error bars are taken as 68 % confidence limit of the PDF. Nevertheless, some other PDFs exhibit other small peaks. They can be due to noise, but they also can be due to other glitch signatures present in the data, especially tiny residuals from the outer layers. To take care of such situations, we also compute $T_{\rm BCZ}$ by isolating the highest peak and fitting it with a Gaussian profile. When the secondary peaks are small enough, the values and associated errors obtained through the two methods are very similar. We have been successful mainly on main-sequence stars, while subgiant stars presenting mixed modes strongly disturb the analysis.

**Table 1.** Basic spectroscopic and seismic data for 19 *Kepler* stars

| KIC ID | $T_{\rm eff}$ (K) | $\log g$ | [Fe/H] | $\Delta_0$ ($\mu$Hz) |
|---|---|---|---|---|
| KIC003632418 | 6190 | 4.01 | −0.19 | 60.5 ± 0.1 |
| KIC004914923 | 5905 | 4.19 | 0.14 | 88.3 ± 0.1 |
| KIC006106415 | 5990 | 4.29 | −0.11 | 103.7 ± 0.1 |
| KIC006116048 | 5935 | 4.27 | −0.26 | 100.3 ± 0.2 |
| KIC006603624 | 5625 | 4.31 | 0.26 | 109.9 ± 0.1 |
| KIC006933899 | 5860 | 4.08 | 0.01 | 71.8 ± 0.1 |
| KIC007976303 | 6053 | 3.90 | −0.52 | 50.9 ± 0.2 |
| KIC008006161 | 5390 | 4.47 | 0.38 | 149.1 ± 0.1 |
| KIC008228742 | 6042 | 4.02 | −0.15 | 61.6 ± 0.1 |
| KIC008379927 | 5960 | 4.39 | −0.30 | 119.9 ± 0.1 |
| KIC008760414 | 5787 | 4.33 | −1.19 | 117.0 ± 0.1 |
| KIC010018963 | 6020 | 3.95 | −0.47 | 55.2 ± 0.2 |
| KIC010454113 | 6120 | 4.32 | −0.07 | 105.1 ± 0.2 |
| KIC010963065 | 6060 | 4.28 | −0.21 | 102.4 ± 0.1 |
| KIC011026764 | 5682 | 3.89 | −0.26 | 50.2 ± 0.1 |
| KIC011244118 | 5745 | 4.07 | 0.34 | 71.3 ± 0.2 |
| KIC011395018 | 5424 | 3.84 | −0.39 | 47.4 ± 0.1 |
| KIC012009504 | 6065 | 4.21 | −0.09 | 87.7 ± 0.1 |
| KIC012258514 | 5990 | 4.12 | 0.02 | 74.5 ± 0.1 |

## 3. Results

We applied the techniques described in Sect. 2 to 19 stars observed by the *Kepler* mission. The frequencies of these stars were given by Appourchaux et al. (2012). While methods A and B and D were applied to all 19 stars, method C was applied to 6 stars. The basic spectroscopic parameters and the average large separation for the stars are given in Table 1. The effective temperatures were adopted from Bruntt et al. (2012) while the $\log g$ values were determined from a seismic pipeline (Basu et al. 2010). The large separation values were obtained from the slope of a linear relation between the radial order and the observed radial mode frequencies used in this study. The position of the 19 stars on the Hertzsprung-Russell diagram are shown in Fig. 5.

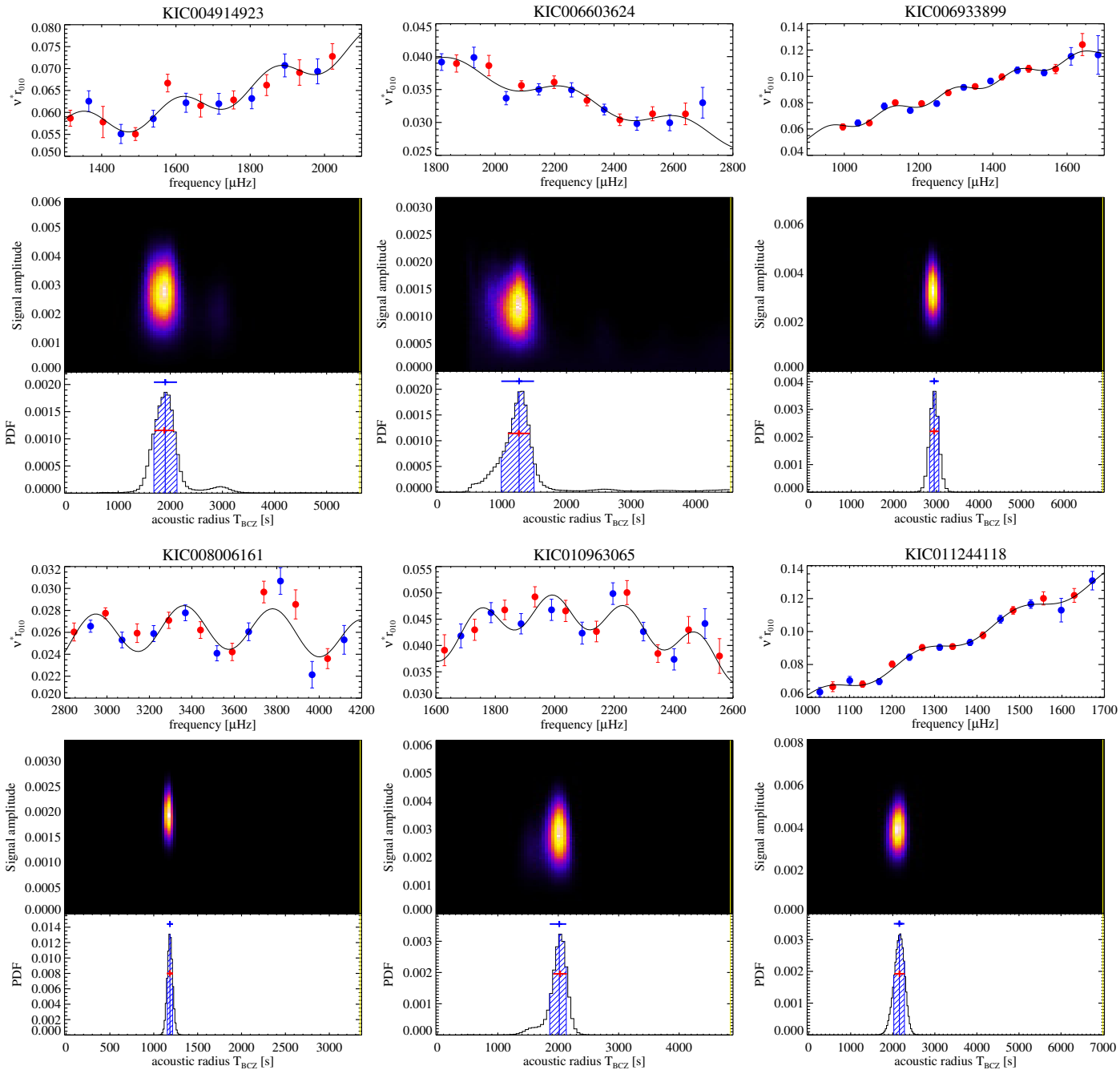


**Fig. 4.** Illustration of method D: Determination of $T_{\rm BCZ}$ using frequency ratios for six *Kepler* targets. Each of the six panels corresponds to a target and is divided into three sub-panels. *Top* sub-panels show the seismic variables $\nu^* r_{010}$. *Blue (red)* dots with error bars are the observed values for $\nu^* r_{01}$ ($\nu^* r_{10}$). *Solid* lines show models (Eq. 19) with the parameters corresponding to the highest posterior probabilities found by MCMC. *Middle* sub-panels are 2-D probability functions in the plane ($T$,$A$). *White (black)* colour corresponds to high (low) probability. *Bottom* sub-panels show marginal probability distributions for the parameter $T$. Vertical *blue* lines indicate the medians of the distributions and hatched areas show the 68%-level confidence intervals. *Blue* error bars, plotted above the peaks, are errors deduced from these intervals, whereas *red* errors, plotted across the peaks, are obtained by fitting the peaks with Gaussian profiles.

We show the results from each method graphically in Figs. 1, 2, 3 and 4 for a selected set of eight stars: KIC004914923, KIC006603624, KIC006933899, KIC008006161, KIC010454113, KIC010963065, KIC011244118, and KIC012009504. Among these, methods A, B and D were applied for all the eight stars, and method C for five stars. However, for methods A and D, not all the cases led to significant results for acoustic depths or radii of BCZ and HeIIZ.

We compare the results for all the 19 stars from all four methods in Table 2. It is to be noted that in this table the acoustic radii of the BCZ ($T_{\rm BCZ}$) determined by method D has been converted to acoustic depths ($\tau_{\rm BCZ}$) through the relation $\tau_{\rm BCZ} = T_0 - T_{\rm BCZ} \approx (2\Delta_0)^{-1} - T_{\rm BCZ}$ for comparison with the values determined by other methods. However, the errors quoted for $\tau_{\rm BCZ}$ from method D are the intrinsic errors from the method, and do not include the errors in $T_0$. Method D did not consider the presence of the HeIIZ signal in the data.

**Table 2.** Comparison of acoustic depths of the base of the convective envelope ($\tau_{\rm BCZ}$) and the second helium ionisation zone ($\tau_{\rm HeIIZ}$) by four independent methods.

| KIC ID | $T_0$ (s) | $\tau_{\rm BCZ}$ (s) | | | | $\tau_{\rm HeIIZ}$ (s) | | |
|---|---|---|---|---|---|---|---|---|
| | | Method A | Method B | Method C | Method D | Method A | Method B | Method C |
| KIC003632418 | 8264 ± 13 | $5199^{+124}_{-124}$ | $5124^{+195}_{-149}$ | | $5062^{+173}_{-173}$ | ··· | $1462^{+69}_{-78}$ | |
| KIC004914923* | 5662 ± 6 | $3744^{+91}_{-91}$ | $3525^{+23}_{-21}$ | | $3777^{+191}_{-191}$ | ··· | $1006^{+25}_{-25}$ | |
| KIC006106415 | 4821 ± 4 | $2903^{+242}_{-242}$ | $2875^{+393}_{-247}$ | | $2811^{+118}_{-118}$ | ··· | $908^{+74}_{-75}$ | |
| KIC006116048 | 4985 ± 9 | $3153^{+220}_{-220}$ | $2942^{+178}_{-273}$ | | $3134^{+186}_{-186}$ | $1015^{+108}_{-108}$ | $1048^{+34}_{-35}$ | |
| KIC006603624* | 4549 ± 4 | $2932^{+183}_{-183}$ | $3234^{+133}_{-438}$ | $3285^{+130}_{-196}$ | $3287^{+171}_{-171}$ | $829^{+89}_{-89}$ | $897^{+36}_{-37}$ | $1031^{+61}_{-96}$ |
| KIC006933899* | 6963 ± 9 | $3773^{+201}_{-201}$ | $4115^{+74}_{-65}$ | $4228^{+675}_{-143}$ | $4014^{+107}_{-107}$ | $1114^{+124}_{-124}$ | $1315^{+54}_{-45}$ | $1721^{+77}_{-64}$ |
| KIC007976303 | 9823 ± 38 | $7026^{+35}_{-35}$ | $6760^{+75}_{-80}$ | | ··· | $2835^{+51}_{-51}$ | $2671^{+33}_{-30}$ | |
| KIC008006161* | 3353 ± 2 | $2284^{+47}_{-47}$ | $2186^{+35}_{-39}$ | $2199^{+40}_{-38}$ | $2169^{+30}_{-30}$ | ··· | $508^{+80}_{-101}$ | $615^{+123}_{-144}$ |
| KIC008228742 | 8116 ± 13 | $4409^{+290}_{-290}$ | $4468^{+89}_{-166}$ | | $4565^{+187}_{-187}$ | ··· | $1509^{+38}_{-46}$ | |
| KIC008379927 | 4170 ± 3 | $1796^{+114}_{-114}$ | $1840^{+29}_{-26}$ | $1858^{+40}_{-38}$ | $(3172^{+61}_{-61})$ | ··· | $714^{+25}_{-27}$ | $827^{+48}_{-57}$ |
| KIC008760414 | 4273 ± 3 | $2750^{+132}_{-132}$ | $2481^{+316}_{-100}$ | | $2430^{+141}_{-141}$ | ··· | $973^{+82}_{-185}$ | |
| KIC010018963 | 9057 ± 32 | $5137^{+310}_{-310}$ | $3820^{+244}_{-357}$ | | ··· | ··· | $1972^{+55}_{-56}$ | |
| KIC010454113* | 4757 ± 9 | $2801^{+125}_{-125}$ | $2949^{+150}_{-26}$ | | ··· | $823^{+18}_{-18}$ | $799^{+14}_{-15}$ | |
| KIC010963065* | 4882 ± 4 | $2832^{+155}_{-155}$ | $2854^{+47}_{-42}$ | $2803^{+120}_{-166}$ | $2852^{+112}_{-112}$ | $1020^{+62}_{-62}$ | $851^{+24}_{-28}$ | $1101^{+27}_{-29}$ |
| KIC011026764 | 9960 ± 19 | $5053^{+33}_{-33}$ | $5048^{+43}_{-38}$ | | ··· | ··· | $2316^{+66}_{-72}$ | |
| KIC011244118* | 7012 ± 19 | $4829^{+251}_{-251}$ | $4844^{+246}_{-133}$ | $4798^{+165}_{-576}$ | $4851^{+125}_{-125}$ | $1490^{+40}_{-40}$ | $1506^{+41}_{-33}$ | $1501^{+88}_{-132}$ |
| KIC011395018 | 10548 ± 22 | $6504^{+276}_{-276}$ | $7223^{+60}_{-57}$ | | ··· | ··· | $3592^{+40}_{-38}$ | |
| KIC012009504* | 5701 ± 6 | $2150^{+74}_{-74}$ | $2174^{+90}_{-288}$ | | ··· | $1039^{+47}_{-47}$ | $1004^{+40}_{-47}$ | |
| KIC012258514 | 6711 ± 9 | $2645^{+151}_{-151}$ | $2819^{+173}_{-338}$ | | ··· | $1277^{+81}_{-81}$ | $1250^{+67}_{-78}$ | |

**Notes.** 1. In method D actually the acoustic *radius*, $T_{\rm BCZ}$ was determined, which has been converted to the corresponding acoustic *depth*, $\tau_{\rm BCZ}$ using the $T_0$ value derived from the average large separation, $\Delta_0$.
2. A blank cell indicates that an estimation of the acoustic depth was not attempted, and a cell with ··· indicates that the estimated value did not pass the applied validity check for the relevant method.
3. Values in parentheses denote a significant detection, but not considered to be associated with an acoustic glitch.
(*) Stars illustrated in Figs. 1–4.

### *3.1. Comparison with stellar models*

The acoustic locations of the glitches determined by all the methods described above do not involve detailed modelling of the stars; they are derived purely from the observed frequencies. In order to check whether the estimated values of $\tau_{\rm BCZ}$ and $\tau_{\rm HeIIZ}$ are consistent with typical stellar models, we carry out a comparison of these with values from representative models of each star. In this, we adopt two approaches. The first one consists of comparing the values with a broad family of models constructed to match the average seismic and spectroscopic properties of the stars to a fair extent. Additionally, we compare our values with the theoretical values of one optimally fitted model for each star.

For this exercise, we compare not the acoustic depths directly, but the fractional acoustic radii of the BCZ and the HeIIZ. This is done for two reasons. Firstly, the acoustic radius is free from the less known contribution to the sound speed from the outermost layers of the stars, and thus should be theoretically a more robust quantity than the acoustic depth. However, in converting the acoustic depth estimated from the oscillatory signal in frequencies to the corresponding acoustic radius we do use the approximate relationship between the total acoustic radius and the large separation. Secondly, by considering the fractional acoustic radii instead of the acoustic radii itself, we remove the effect of overall scaling of the models at slightly different masses and radii. Of course, the change in the relative position of the BCZ and the HeIIZ inside the star reflects a true departure of the models from the observed star.

#### 3.1.1. Comparison with neighbourhood models

In this approach, we consider a broad family of theoretical models which mimic the global properties of the stars and their seismic properties, as listed in Table 1, but cannot be claimed to necessarily have frequencies that match the observed ones very

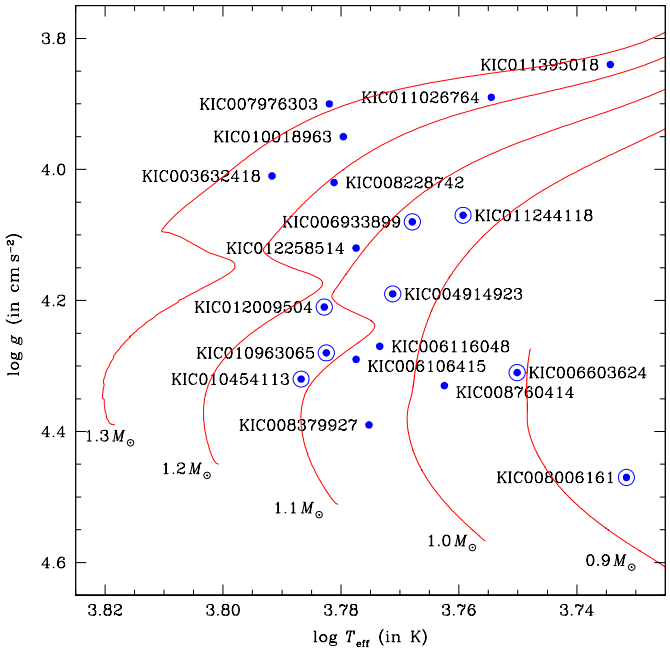


**Fig. 5.** Hertzsprung-Russell diagram for 19 *Kepler* stars. The eight stars discussed in detail are circled. The *red* lines are evolutionary tracks with solar chemical composition and indicated mass.

closely. We deliberately span a very liberal range in each of the global properties. This is because our aim here is to only determine the possible range in the locations of the acoustic glitches in stellar models similar to the target star, and compare the values estimated through the above four methods. Further, we repeat the exact procedure of one of the methods (B) to obtain the acoustic depths $\tau_{\rm BCZ}$ and $\tau_{\rm HeIIZ}$ from the theoretical frequencies of the stellar models. This allows us also to investigate possible systematic shifts between the theoretical acoustic locations of the glitches from the models and their estimated values from the oscillatory signal in the model frequencies themselves.

We used the Yale Stellar Evolution Code (YREC; Demarque et al. 2008) to model the stars. The input physics included the OPAL equation of state (Rogers & Nayfonov 2002) and the OPAL high-temperature opacities (Iglesias & Rogers 1996) supplemented with low-temperature opacities from Ferguson et al. (2005). All nuclear reaction rates were from Adelberger et al. (1998), except for the rate of the $^{14}$N$(p,\gamma)^{15}$O reaction, which was fixed at the value of Formicola et al. (2004). Core overshoot of $0.2H_p$ was included where relevant. For the stars that did not have very low metallicities, we included the diffusion and settling of helium and heavy elements. This was done as per the prescription of Thoul et al. (1994).

The first step of our modelling was to use the average large separation $\Delta_0$ and the frequency of maximum power, $\nu_{\rm max}$, along with $T_{\rm eff}$ and metallicity to determine the masses of the stars using a grid-based Yale-Birmingham pipeline (Basu et al. 2010; Gai et al. 2011). We use four grids for this: the models from the Yonsei-Yale (YY) isochrones (Demarque et al. 2004), and the grids of Dotter et al. (2008),Marigo et al. (2008) and Gai et al. (2011). Mathur et al. (2012) have shown that grid-based estimates of stellar masses and radii agree very well with those obtained from more detailed modelling of the oscillation frequencies of stars.

For each star, we specified 8–12 initial masses scanning a $2\sigma$ range on either side of the mass obtained by the grid modelling. For each initial mass we modelled the star using three values of the mixing length parameter $\alpha$ (1.826, 1.7 and 1.5; note $\alpha$ = 1.826 is the solar calibrated value of $\alpha$ for YREC). For each value of mass and $\alpha$ we assumed at least four different values of the initial helium abundance $Y_0$. In general $Y_0$ ranged from 0.25 to 0.30. The models were evolved from ZAMS and the properties were output at short intervals to allow us to calculate oscillation frequencies for the model as it evolved.

All models satisfying the observed constraints on large separation, small separation, $T_{\rm eff}$, $\log g$ and [Fe/H] were selected for comparison. In order to get a reasonably large number of models the error margin was assumed to be 2.0 $\mu$Hz, 2.0 $\mu$Hz, 200 K, 0.1 dex and 0.1 dex respectively. The number of models selected with this criterion ranged from about 80 to 800. For each of these models, the acoustic depths $\tau_{\rm BCZ}$ and $\tau_{\rm HeIIZ}$ were determined by a procedure exactly similar to method B adopted for the real data. The theoretically computed value of the frequency was taken as the mean value and the uncertainty of the corresponding mode frequency in the *Kepler* data of the concerned star was adopted as the error. Thus, the model data set mimicked the observed data set in terms of number of modes, specific modes used in the fitting and the errorbars on the frequencies.

The comparison of the fractional acoustic radii of the glitches in the models and our estimates from the *Kepler* data are shown in Fig. 6. In this figure we show the values obtained by the different methods by coloured symbols. The acoustic depths obtained by methods A, B, and C have been converted to acoustic radii through the relation $t = T_0 - \tau \approx (2\Delta_0)^{-1} - \tau$. The errorbars on the values from these methods include the uncertainty propagated in the calculation of $T_0$ from $\Delta_0$, as listed in Table 2. The figure shows the calculated values of the acoustic radii of the glitches from the models as well as their estimates from the second differences of the frequencies obtained by method B. For the latter, the typical error (not shown in the graphs for the sake of clarity) would be similar to that of the values obtained from the *Kepler* data by the same method, since we have assumed the same uncertainties on the theoretical frequencies as the data.

### 3.1.2. Comparison with optimally fitted models

We also compare our estimated acoustic locations of the glitches to those in an optimally fitted model of each star. The fitted model was obtained through the Asteroseismic Modelling Portal (AMP), the details of which can be found in Mathur et al. (2012). The AMP model values are listed in Table 3 and, for seven of the selected stars, shown in Fig. 6.

## 4. Discussion

Overall we find remarkably good agreement between the values of the acoustic depths of the BCZ determined by different methods. In most cases the $\tau_{\rm BCZ}$ (or the corresponding $T_{\rm BCZ}$) agree with each other well within the quoted $1\sigma$ error bars (cf. Table 2).

The location of the HeIIZ turns out to be more difficult to determine from the frequencies directly (method A). This is probably because of the interplay of the smooth trend in frequencies with the slowly varying oscillatory signal from the HeIIZ. Even the general agreement between $\tau_{\rm HeIIZ}$ values from different methods is not as good as those for $\tau_{\rm BCZ}$, although it is mostly within $1\sigma$ uncertainties, nevertheless.

While comparing our estimates of the acoustic depths $\tau_{\rm BCZ}$ and $\tau_{\rm HeIIZ}$ from methods A, B and C to the acoustic radii from

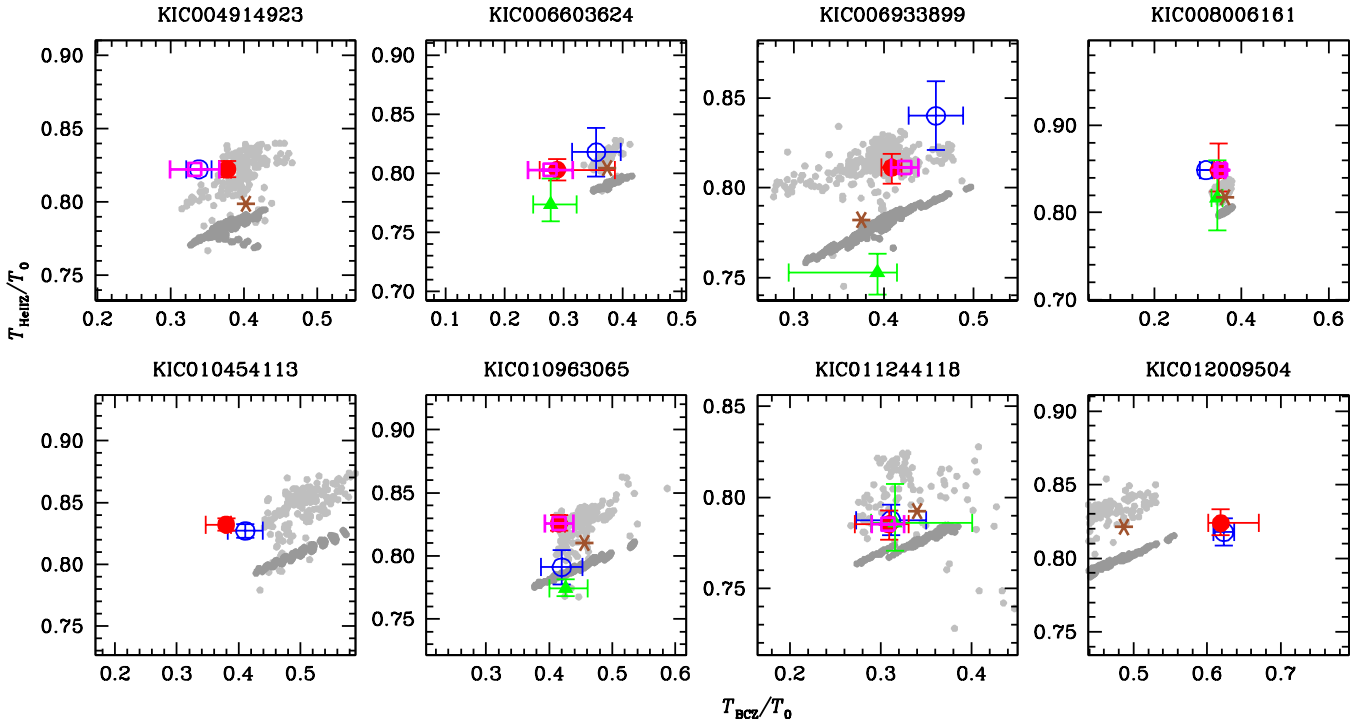


**Fig. 6.** Comparison of fractional acoustic radii $T_{\rm BCZ}/T_0$ and $T_{\rm HeIIZ}/T_0$ determined from the oscillatory signal in the *Kepler* frequencies of 8 stars by up to four methods (*blue empty circle* for A, *red filled circle* for B, *green filled triangle* for C and *magenta empty square* for D, each with errorbars) with corresponding values from representative models of the stars. For methods A and D, in cases where $T_{\rm HeIIZ}$ was not determined, its value has been provided by the $T_{\rm HeIIZ}$ value determined by method B. The *dark grey circles* indicate the actual value of the fractional acoustic radii in the stellar models, while the *light grey dots* represent the values of the fractional acoustic radii determined from the theoretical frequencies of the models by method B. The *brown asterisk* indicates the AMP model. For each star, the ranges of each axis shown in the graph correspond to $\pm 1000$ s and $\pm 500$ s of the values of $T_{\rm BCZ}$ and $T_{\rm HeIIZ}$ determined by method B, respectively.

method D, or from typical models, we invoke the relationship between the total acoustic radius $T_0$ and the average large separation $\Delta_0$, i.e., $T_0 \approx (2\Delta_0)^{-1}$. This relationship is an approximate one. Further, the observed average large separation, $\Delta_0$ depends on the adopted frequency range over which it is measured and also on the adopted method. There are at least three different methods available in the literature for determining the observed value of $\Delta_0$: (1) from taking a mean value over some arbitrarily chosen frequency range for modes of like degree $l$, (2) from determining the frequency of the corresponding spectral peak in the Fourier spectrum of the power spectrum of the observed oscillations, (3) from fitting the asymptotic expression for solar-like oscillations (Tassoul 1980; Gough 1986) to the observed frequencies. Here we have calculated $\Delta_0$ by fitting a linear relation to the observed radial mode frequencies as a function of the radial order, which is equivalent to the third method above. In principle, an estimation of $T_0$ from $\Delta_0$ measured by another alternative technique will yield a slightly different value. However, given that the large separation is a fairly robust quantity, especially for stars with high signal to noise ratio (see Verner et al. 2011), we do not expect this to be a major source of uncertainty.

However, particular attention should be paid to the systematic biases involved in treating the outermost layers of the star by different seismic diagnostics dealing with the determination of acoustic depths of glitches. Although one may hope that the different methods (seismic diagnostics) will provide similar stellar radii $r$ for the acoustic glitches of both the helium ionisation zones and the base of the surface convection zone, the seismically measured acoustic depths $\tau(r)$ of these glitches will in general be different, for they depend on the very details of the adopted seismic diagnostic. For example, method C approximates the outer stellar layers by a polytrope with a polytropic index $m = 3.5$, allowing for some account of the location of the outer turning point of an incident acoustic wave by approximating the acoustic cutoff frequency $\nu_{\rm ac} \simeq (m+1)/\tau$ (Houdek & Gough 2007). An incident wave, approaching the upper turning point, would sense a location of the seismic surface on which the sound speed $c = c_0\tau$ (where $c_0$ is a constant), if extrapolated linearly outwards with respect to acoustic depth $\tau(r)$ from the outer layers of the adiabatically stratified region of the convection zone, would vanish (Balmforth & Gough 1990; Lopes & Gough 2001). This location, lying well inside the evanescent zone of most of the acoustic modes, simply acts as a (virtual) singularity in the acoustic wave equation, providing a convenient fiducial location with respect to which the acoustic phase in the propagating zone beneath is related (Gough 2012). In a solar model the so-determined location of the seismic surface is about 111 s in acoustic height above the temperature minimum (Lopes & Gough 2001), or some 225 s in acoustic height above the photosphere (Houdek & Gough 2007). Consequently the acoustic depths, but not necessarily the corresponding radii $r$, of the acoustic glitches will be larger when determined with a seismic diagnostic, such as method C, that takes explicit account of the upper turning point in some approximate way.

In Table 2 and Fig. 6 we did not take account of these differences in the acoustic depths between the methods A, B and C and the calculated stellar models. Only a careful analysis of properly calibrated stellar models would provide these differences in the

**Table 3.** Acoustic radii of glitches in AMP models. Total acoustic radii of the stars in the AMP models and as estimated from the average large separation are also given.

| KIC ID | $T_{\rm BCZ}$ (s)[a] | $T_{\rm HeIIZ}$ (s)[a] | $T_0$ (s)[a] | $T_0$ (s)[b] |
|---|---|---|---|---|
| KIC003632418 | 4289 | 6517 | 7911 | 8264 ± 13 |
| KIC004914923* | 2177 | 4322 | 5410 | 5662 ± 6 |
| KIC006106415 | 2003 | 3735 | 4623 | 4821 ± 4 |
| KIC006116048 | 2019 | 3844 | 4779 | 4985 ± 9 |
| KIC006603624* | 1629 | 3503 | 4356 | 4549 ± 4 |
| KIC006933899* | 2488 | 5188 | 6633 | 6963 ± 9 |
| KIC007976303 | 4012 | 7240 | 9305 | 9823 ± 38 |
| KIC008006161* | 1177 | 2647 | 3239 | 3353 ± 2 |
| KIC008228742 | 3724 | 6278 | 7746 | 8116 ± 13 |
| KIC008379927 | 1780 | 3285 | 4019 | 4170 ± 3 |
| KIC008760414 | 1675 | 3229 | 4084 | 4273 ± 3 |
| KIC010963065* | 2128 | 3787 | 4673 | 4882 ± 4 |
| KIC011026764 | 3103 | 7303 | 9459 | 9960 ± 19 |
| KIC011244118* | 2286 | 5330 | 6726 | 7012 ± 19 |
| KIC012009504* | 2660 | 4485 | 5461 | 5701 ± 6 |
| KIC012258514 | 2761 | 5170 | 6410 | 6711 ± 9 |

[a] Calculated from AMP model
[b] Estimated from $\Delta_0$ of *Kepler* data
(*) Stars illustrated in Figs. 1–4.

locations of the seismic surfaces; this, however, is beyond the scope of the present paper.

We also notice a systematic shift in the acoustic radius of the HeIIZ in a stellar model and its estimated value from the oscillatory signal in the model frequencies, at least, by method B. The fitted value of $\tau_{\rm HeIIZ}$ is typically lower than the model value by about 100 s, on average. This is a generic feature of nearly all the stars (see Fig. 6) and might have its roots in the treatment of the acoustic surface, as discussed above. However, we do not find such a systematic shift between the $\tau_{\rm BCZ}$ values of the models and the fits.

The $T_0$ values of AMP models are systematically smaller (by about 200 s, on average) than those estimated from $\Delta_0$ of the *Kepler* data used in this paper. However, the AMP fitting has been subjected to the surface correction technique (Mathur et al. 2012), while the present data have not been.

### 4.1. Discussion of specific cases

We discuss the cases of the eight selected stars in detail below. The cases of the 11 remaining stars are somewhat similar to these and a general understanding of the issues involved may be obtained from the selected subsample itself.

#### 4.1.1. KIC004914923

The $\tau_{\rm BCZ}$ values for this star have been obtained by methods A, B and D, and the values agree just within $1\sigma$ uncertainties. The PDF in method D shows a very small secondary peak at $T_{\rm BCZ} \sim 3000$ s, but the histogram for $\tau_{\rm BCZ}$ in method B shows no such feature. The histogram for $\tau_{\rm HeIIZ}$ in method B is sharply peaked, producing a definite determination of the acoustic depth of HeIIZ, but $\tau_{\rm HeIIZ}$ could not be determined from method A. The derived values for $T_{\rm BCZ}$ and $T_{\rm HeIIZ}$ agree quite well with those derived from the model frequencies, as well as the AMP model values.

#### 4.1.2. KIC006603624

The oscillatory signal from the BCZ for this star seems to be weaker in comparison to the signal from the HeIIZ, as borne out in each of Figs. 1–4. In Fig. 1, the amplitude of the oscillations in $\delta_{\rm BCZ}$ does not exceed $0.1\,\mu$Hz, lower than all the other stars shown. It is therefore, somewhat difficult to determine the acoustic location of the BCZ. This is reflected in the wider and flatter peaks in the histogram in method B (see Fig. 2), the PDF in method D (see Fig. 4), and the larger errorbars from all the four methods. However, the median values of $\tau_{\rm BCZ}$ derived from all the methods agree quite well. The values of $\tau_{\rm HeIIZ}$ obtained from methods A and B agree with each other, but only at $2\sigma$ level with that from method C. The agreement with model values is barely at $1\sigma$ for $T_{\rm BCZ}$ but well within $1\sigma$ for $T_{\rm HeIIZ}$. The AMP model is also consistent with the other models.

#### 4.1.3. KIC006933899

The $\tau_{\rm BCZ}$ values from all methods agree well within $1\sigma$, and the $\tau_{\rm HeIIZ}$ determined from methods A and B also do barely within $1\sigma$. However, $\tau_{\rm HeIIZ}$ from method C is more than $2\sigma$ deeper. While the model values of $T_{\rm BCZ}$ agree very well with all the derived values, the $T_{\rm HeIIZ}$ from methods A and B match the model fitted values while that from method C is close to the actual model value. The AMP model also lies in the vicinity of the other models.

#### 4.1.4. KIC008006161

This is one of the easiest cases for the determination of $\tau_{\rm BCZ}$ or $T_{\rm BCZ}$, and all the methods converge to one consistent value which also agrees with the models. The determination of $\tau_{\rm HeIIZ}$ from method A did not produce a consistent result, and hence was rejected. Methods B and C agree with the model values, as well as the AMP value.

#### 4.1.5. KIC010454113

This star was attempted by only two methods, A and B, and they produce consistent results for both BCZ and HeIIZ. The model values also lie close to these. This case illustrates the problem of aliasing encountered while fitting the oscillatory signal due to BCZ. This is reflected in the dual peaks in the histogram of method B (Fig. 2).

#### 4.1.6. KIC010963065

All the four methods provide almost identical determinations of $\tau_{\rm BCZ}$ (or corresponding $T_{\rm BCZ}$), but the $\tau_{\rm HeIIZ}$ determined from

method B agrees with those from the other two methods only at $2\sigma$ level. However, the model values span the range of the determined $T_{\rm HeIIZ}$.

#### 4.1.7. KIC011244118

This is a relatively evolved star, for which there are possibly three mixed dipole modes. Once these modes are removed from consideration, all the four methods produce exceptionally close median values of both $\tau_{\rm BCZ}$ ($T_{\rm BCZ}$) and $\tau_{\rm HeIIZ}$ ($T_{\rm HeIIZ}$), even though the uncertainties are large in the former. The model fitted values have a larger scatter possibly because the radial orders of the mixed modes were not identical in such a wide range of models, and thus those were not all removed during fitting.

#### 4.1.8. KIC012009504

Only two methods, A and B, were applied for this star. Although in method B, we observed three peaks in the histogram for $\tau_{\rm BCZ}$, they cannot be explained as an aliasing artefact. Nevertheless, the highest peak value agrees very well with that from method A. The $\tau_{\rm HeIIZ}$ values obtained by the two methods also are consistent. However, the model values of $T_{\rm BCZ}$ seem to be smaller than our derived values. This is possibly due to inadequacy of the model to mimic the real star, rather than a genuine discrepancy. However, the AMP model also does not match our values.

#### 4.1.9. Other discrepant cases

For the remaining 11 stars in the sample, the four methods agree remarkably well for most cases. Some discrepancies do occur for KIC007976303, KIC008379927, KIC010018963, KIC011395018, and KIC012258514.

KIC007976303 is an evolved star for which only 23 frequencies could be used, and even some of these modes could be mixed in nature. Neither the $\tau_{\rm BCZ}$ nor the $\tau_{\rm HeIIZ}$ values determined from methods A and B agree for this star.

For KIC008379927, the first three methods produce consistent results for $\tau_{\rm BCZ}$. Method D does produce a pronounced peak in the PDF, but at a value which is unlikely to correspond to the location of BCZ. A determination of $\tau_{\rm HeIIZ}$ for this star was only possible from methods B and C which agree to within $1.5\sigma$.

KIC010018963 seems to be a case where methods A and B have determined the mutually aliased values of $\tau_{\rm BCZ}$, and it is difficult to choose one over the other as the likely correct location of the BCZ.

KIC011395018 is a sub-giant star with several mixed modes, and it is therefore hardly surprising that methods A and B have failed to produce consistent values of $\tau_{\rm BCZ}$.

## 5. Summary

We have utilised the oscillatory signal in the frequencies of 19 *Kepler* stars to determine the location of the two major acoustic glitches in the stellar interior, namely, the base of the convection zone and the second helium ionisation zone. Four independent approaches were used which exploited the presence of the signal in the frequencies themselves, the second differences of the frequencies and the ratio of small to the large separation. For the stars where more than one method were applied, we found remarkable agreement in the results, in general. There were, however, a few discrepant cases, some which could be traced to the issue of aliasing between the acoustic depth and radius of the glitch. In some others, the presence of mixed modes prevented an accurate analysis.

As a sanity check on the values of the acoustic radii of the acoustic glitches determined from the observed frequencies of a star, we also compared them with theoretical model values. For each star, a large number of representative models were constructed and the same method applied for the theoretical frequencies of these as was done for the observed frequencies. For most of the stars the estimated location of the glitches were found to be in close agreement with the model values, within errorbars.

The present work demonstrates the viability of the techniques applied to determine the acoustic location of layers of sharp variation of sound speed in the stellar interior. These methods thus provide powerful tools for placing strict constraints on the stratification inside solar-type stars (Mazumdar 2005). With the availability of precise frequency sets for a large number of stars from the *Kepler* mission, one can use these techniques to follow the variation of the location of acoustic glitches in a large ensemble of solar-type stars populating the main sequence and sub-giant branches. Further, the amplitude of the oscillatory signal due to the second helium ionisation zone can provide an estimate of the helium content in the stellar envelope (Basu et al. 2004). Such studies are envisaged as the follow-up of the present work.

*Acknowledgements.* AM acknowledges support from the National Initiative on Undergraduate Science (NIUS) undertaken by the Homi Bhabha Centre for Science Education – Tata Institute of Fundamental Research (HBCSE-TIFR), Mumbai, India. JB acknowledges Othman Benomar for useful advice on MCMC methods. GH acknowledges support by the Austrian Science Fund (FWF) project P21205-N16.

## References

Adelberger E. G., Austin, S. M., Bahcall, J. N., et al. 1998, Rev. Mod. Phys., 70, 1265
Appourchaux, T., Chaplin, W. J., García, R. A., et al. 2012, arXiv:1204.3147, accepted in A&A
Ballot, J., Turck-Chièze, S., & García, R. A. 2004, A&A, 423, 1051
Balmforth N. J. & Gough D. O. 1990, ApJ, 362, 256
Basu, S. 1997, MNRAS, 288, 572
Basu, S., Antia, H. M., & Narasimha, D. 1994, MNRAS, 267, 209
Basu, S., Mazumdar, A., Antia, H. M., & Demarque, P. 2004, MNRAS, 350, 277
Basu, S., Chaplin, W. J., Elsworth, Y. 2010, ApJ, 710, 1596
Benomar, O., Appourchaux, T., & Baudin, F. 2009, A&A, 506, 15
Borucki W. J. et al. 2010, Sci, 327, 977
Bruntt, H., Basu, S., Smalley, B., et al. 2012, MNRAS, 423, 122
Christensen-Dalsgaard, J., Monteiro, M. J. P. F. G., Thompson, M. J. 1995, MNRAS, 276, 283
Cunha, M. S., & Brandão, I. M. 2011, A&A, 529, A10
Demarque, P., Woo, J.-H., Kim, Y.-C., & Yi, S. K. 2004, ApJS, 155, 667
Demarque, P., Guenther, D. B., Li, L. H., Mazumdar, A., & Straka, C. W. 2008, Ap&SS, 316, 31
Dotter, A., Chaboyer, B., Jevremovic, D. et al. 2008, ApJ, 178, 89
Ferguson, J. W., Alexander, D. R., Allard, F., et al. 2005, ApJ, 623, 585
Formicola A., Imbriani, G., Costantini, H. et al. 2004, Physics Letters B, 591, 61
Gai, N., Basu, S., Chaplin, W. J., Elsworth, Y. 2011, ApJ, 730, 63
García, R. A., Hekker, S., Stello, D., et al. 2011, MNRAS, 414, L6
Gilliland, R. L., Jenkins, J. M., Borucki, W. J., et al. 2010, ApJ, 713, L160
Gough D. O. 1986, in Hydrodynamic and Magnetodynamic Problems in the Sun and Stars, Y. Osaki (ed.), Univ. Tokyo Press, 117
Gough, D. O. 1990, Progress of Seismology of the Sun and Stars, 367, 283
Gough D. O. 2002, in Proceedings of the First Eddington Workshop on Stellar Structure and Habitable Planet Finding, B. Battrick, F. Favata, I. W. Roxburgh & D. Galadi, eds, ESA SP-485, Noordwijk: ESA, p. 65
Gough D. O. 2012, submitted to PASP
Gough, D. O., & Sekii, T. 1993, in GONG 1992: Seismic Investigation of the Sun and Stars, T. M. Brown (ed.), ASP Conf. Ser. Vol. 42., Astron. Soc. Pac., San Francisco, p. 177
Handberg, R., & Campante, T. L. 2011, A&A, 527, A56

Houdek04, G. 2004, in Equation-of-state and Phase-transition Issues in Models of Ordinary Astrophysical Matter. V. Celebonovic, W. Däppen, D. O. Gough, eds, AIP Conf. Proc., Vol. 731, AIP, New York, p. 193
Houdek, G., Gough, D. O. 2004, in Proc. SOHO 14/GONG 2004: Helio- and Asteroseismology: Towards a Golden Future, Danesy D., ed., ESA SP-559, Noordwijk, p. 464
Houdek, G., Gough, D. O. 2007, MNRAS, 375, 861
Houdek, G., Gough, D. O. 2011, MNRAS, 418, 1217
Iglesias, C. A., Rogers, F. J. 1996, ApJ, 464, 943
Koch D. G. et al. 2010, ApJ, 713, L79
Lopes I. P. & Gough D. O. 2001, MNRAS, 322, 473
Marigo, P., Girardi, L., Bressan, A. et al. 2008, A&A, 482, 883
Mathur, S., Metcalfe, T. S., Woitaszek, M. et al. 2012, ApJ, 749, 152
Mazumdar, A. 2005, A&A, 441, 1079
Mazumdar, A., & Antia, H. M. 2001, A&A, 377, 192
Mazumdar, A., Michel, E., Antia, H. M., Deheuvels, S. 2012, A&A, 540, A31
Miglio, A., Montalbán, J., Carrier, F., et al. 2010, A&A, 520, L6
Monteiro, M. J. P. F. G., Christensen-Dalsgaard, J., Thompson, M. J. 1994, A&A, 283, 247
Monteiro, M. J. P. F. G., & Thompson, M. J. 1998, in Korzennik, S. G., Wilson, A., eds, Structure and Dynamics of the Interior of the Sun and Sun-like Stars. ESA Publications Division, ESA Special Publications, 418, 819
Monteiro, M. J. P. F. G., Christensen-Dalsgaard, J., Thompson, M. J. 2000, MNRAS, 316, 165
Monteiro, M. J. P. F. G., & Thompson, M. J. 2005, MNRAS, 361, 1187
Rogers, F. J., Nayfonov, A. 2002, ApJ, 576, 1064
Roxburgh, I. W. 2005, A&A, 434, 665
Roxburgh, I. W. 2009, A&A, 493, 185
Roxburgh, I. W. & Vorontsov, S. V. 1994, MNRAS, 268, 880
Roxburgh, I. W. & Vorontsov, S. V. 2003, A&A, 411, 215
Silva Aguirre, V., Ballot, J., Serenelli, A. M., & Weiss, A. 2011, A&A, 529, A63
Tassoul M. 1980, ApJS, 43, 469
Thoul A. A., Bahcall J. N., Loeb A. 1994, ApJ, 421, 828
Verner, G. A., Elsworth, Y., Chaplin, W. J., et al. 2011, MNRAS, 415, 3539